Supporting Information

Construction of the donor-acceptor type conjugated porous polymer/g-C_3N_4 S-scheme heterojunction for efficient photocatalytic hydrogen production

Yinfeng Han, [†*a,] Miao Liu,[†b] Aihuan Sun,[a] Fei Zhao,[*a] Jinsheng Zhao[b] and ChangAn Wang[*a]

[a]College of Chemistry and Chemical Engineering, Taishan University, Taian, 271000, PR China.
[b]Shandong Key Laboratory of Chemical Energy Storage and Novel Cell Technology, College of Chemistry and Chemical Engineering, Liaocheng University, Liaocheng, 252059, China.
[†]The authors contribute equally to this work.

Corresponding Authors: han@tsu.edu.cn, zhaofei@tsu.edu.cn, and wangcha@tsu.edu.cn

1. Experimental section

1. 1. Chemicals and reagents

2,2'-(5,5'-(2,6-Bis(4,4,5,5-tetramethyl-1,3,2-dioxaborolan-2-yl)benzo[1,2-b:4,5-b']dithiophene-4,8-diyl)bis(thiophene-5,2-diyl))bis(4,4,5,5-tetramethyl-1,3,2-dioxaborolane), 3,7-dibromodibenzothiophene-5,5-dioxide, tetrakis(triphenylphosphine)palladium(0) ($Pd(PPh_3)_4$) were obtained from Zhengzhou Alfachem Co., Ltd. N-methypyrrolidone (NMP), ascorbic acid (AA, AR grade), ethanol, chloroform, N,N-dimethylformamide (DMF), potassium carbonate, 5,5-dimethyl-1-pyrroline N-oxide (DMPO) were bought from Aladdin Co., LTD. The above purchased samples and reagents were used without further purification.

2. Characterization

2.1. The instrumental analysis method

Solid state magic angle spinning ^{13}C CP-MAS NMR measurement was performed on a Bruker Avance III HD 600 MHz wide Bore Solid NMR spectrometer at a MAS rate of 10 kHz. Fourier transform infrared (FT-IR) spectra were measured on a Nicolet Avatar 360

FT-IR spectrometer. X-ray diffraction (XRD) curves of samples were measured from 5° to 80° by X-ray powder diffractometer (Smart Lab 9kW). The thermogravimetric data of samples were measured on Netzsch TA449F5-QMS403D thermal analyzer between 20 °C and 800 °C under nitrogen atmosphere. The surface chemical states of sample were carried out by X-ray photoelectron spectroscopy (XPS) were recorded on ESCALAB 250Xi spectrometer. Scanning electron microscope (SEM) (Thermo Fisher Scientific FIB-SEM GX4) was used to measure the morphology of materials. The element distribution and composition of photocatalyst were preliminarily evaluated by Scanning electron microscope energy dispersive spectrometer (SEM-EDS). Surface areas and pore size distributions were measured by Nitrogen isotherm adsorption-desorption at 77.3 K through ASAP 2460-3 (Micromeritics) volumetric adsorption analyzer. The UV-Vis absorption spectroscopy of polymers was measured by Varian Carry 5000 UV-VIS-NIR spectrometer. Photoluminescence (PL) emission spectra were collected on an F-7000 FL spectrophotometer. The Electron paramagnetic resonance spectroscopy was measured on China instru&Quantumtech (Hefei) EPR200-Plus with continues-wave X band frequency. Ultraviolet photoelectron spectroscopy (UPS) was performed on ThermoFischer ESCALAB 250Xi spectrometer with a He discharge lamp (He I, 21.22 eV) [S1].

2.2. Electrochemical measurements

Electrochemical impedance spectra (EIS) were measured on a CHI660E (Chenhua, Shanghai) electrochemical workstation with a standard three-electrode system (the sample modified Pt-disk electrode as the working electrode, Pt flake and Ag/AgCl as the counter electrode and reference electrode, respectively). Firstly, the catalyst slurry was prepared, which consists of photocatalyst sample (10 mg), isopropyl alcohol (1 mL) and 30 μL nafion, then be dispersed ultrasonically in an ultrasonic bath. Then 10 μL of the catalyst slurry was dropped on the platinum plate electrode (Φ 3 mm) and dried under an infrared lamp before the measurement. EIS were measured in a frequency range from 0.01 Hz to 100 k Hz at 0.2 V, and Na_2SO_4 aqueous solution (0.5 M) was used as the electrolyte.

2.3. Transient photocurrent measurements

The transient photocurrent responses (I-t) were also measured on CHI 760C (CH Instruments Inc., U.S.A.) electrochemical workstation in a standard three-electrode system, including a Pt sheet as the counter electrode (1 cm × 1 cm), an Ag/AgCl electrode as the reference electrode, and a catalyst-modified indium tin oxide (ITO) electrode as the working electrode. An 0.5 M Na_2SO_4 aqueous solution was used as an electrolyte. The catalyst slurry was prepared by adding 10 mg of catalyst to a mixture solution of 1 mL isopropyl alcohol and 30 μL Nafion (5%), and the slurry was fully dispersed in an ultrasonic cleaner for 30 min before use. For the preparation of the ITO electrode, 20 μL of the above polymer slurry was coated on the ITO/glass electrode with a surface area of 1 cm × 1 cm and dried in an oven at 80 ℃[S2].

2.3. AQY measurements

The apparent quantum yields (AQY) of samples were measured under monochromatic light. The selected wavelengths were 380, 420, 475, 550 and 600 nm with the intensities of 8.73, 36.6, 60.8, 72 and 55.6 mW/cm^2, respectively. The AQY was calculated according to following equation [S3, S4]:

$$\mathrm{AQY}=\frac{Ne}{Np}*100\% = \frac{2*M*NA*h*c}{S*P*t*\lambda}*100\%$$

where M is the amount of H_2 (mol), N_A is Avogadro constant (6.02 × 10^{23} mol^{-1}), h is the Planck constant (6.626 × 10^{-34} J/s), c is the speed of light in vacuum (3 × 10^8 m/s), S is the irradiation area (19.6 cm^2 in our experiment), P is the intensity of irradiation light (W/cm^2), t is the irradiation time (s), λ is the wavelength of monochromatic light (m).

3. Theoretical section

In this work, we employed Vienna ab initio simulation package (VASP) [S5] to investigated the geometry and electronic properties of the DBDSO/CN heterojunction. The Perdew-Burke-Erzerhof (PBE) functional within the generalized gradient approximation (GGA) was adopted to deal with the exchange-correlation functionals [S6-S7]. Convergence criteria for energy and force were set as 10^{-6} eV and 0.03 eV/Å,

respectively. The electronic wave function uses a cutoff energy of 550 eV. A vacuum space in the z-direction more than 15 Å was added to avoid the neighboring slab interactions. The Brillouin zone was sampled by a Gamma-centered k-point grid of 2 × 1 × 1 for the structural optimization and 3 × 2 × 1 for the calculations of the electronic properties, respectively. In order to describe the van der Waals force precisely, the DFT-D3 method improved by Grimme et al. was considered.

To assess the stabilities of the heterostructures, the interface binding energies were calculated by the following equation:

$$E_b = (E_{DBDSO/CN} - E_{CN} - E_{DBDSO})/S$$

where $E_{DBDSO/CN}$, E_{CN}, and E_{DBDSO} represent the total energies of the DBDSO/CN, CN, and DBDSO, respectively, and S is the surface area of the supercell. The lower E_b value means better stability of the heterostructure.

The charge transfer and redistribution can be characterized by the work function:

$$\Phi = E_{vac} - E_F$$

where E_{vac} and E_F represent vacuum and Fermi level, respectively.

4. Results and discussion

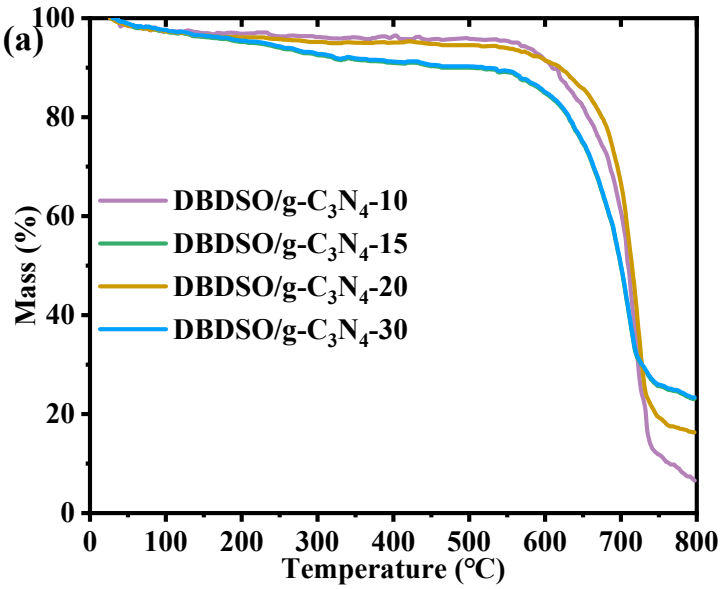

Fig. S1 Thermogravimetric curves of DBDSO/g-C_3N_4-x.

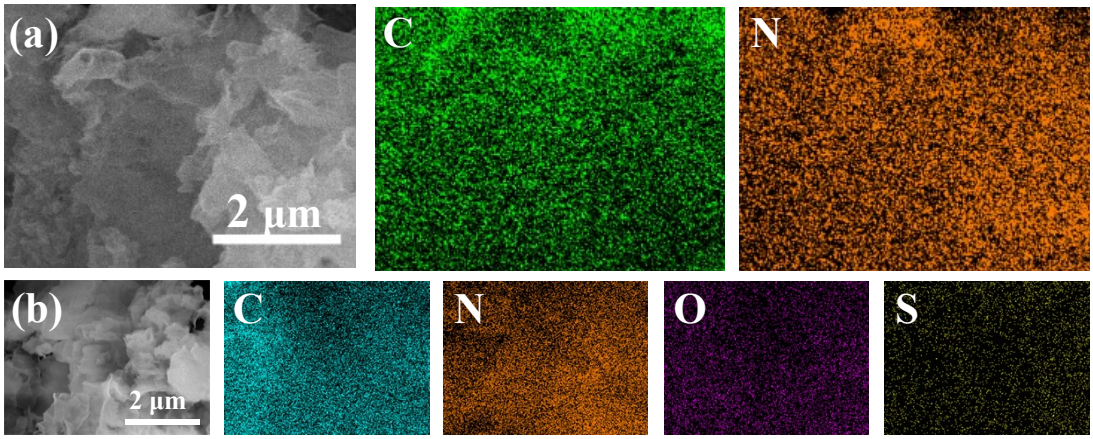

Fig. S2 The elemental mapping images of CN (a), DBDSO/g-C_3N_4-15 (b) after irradiation.

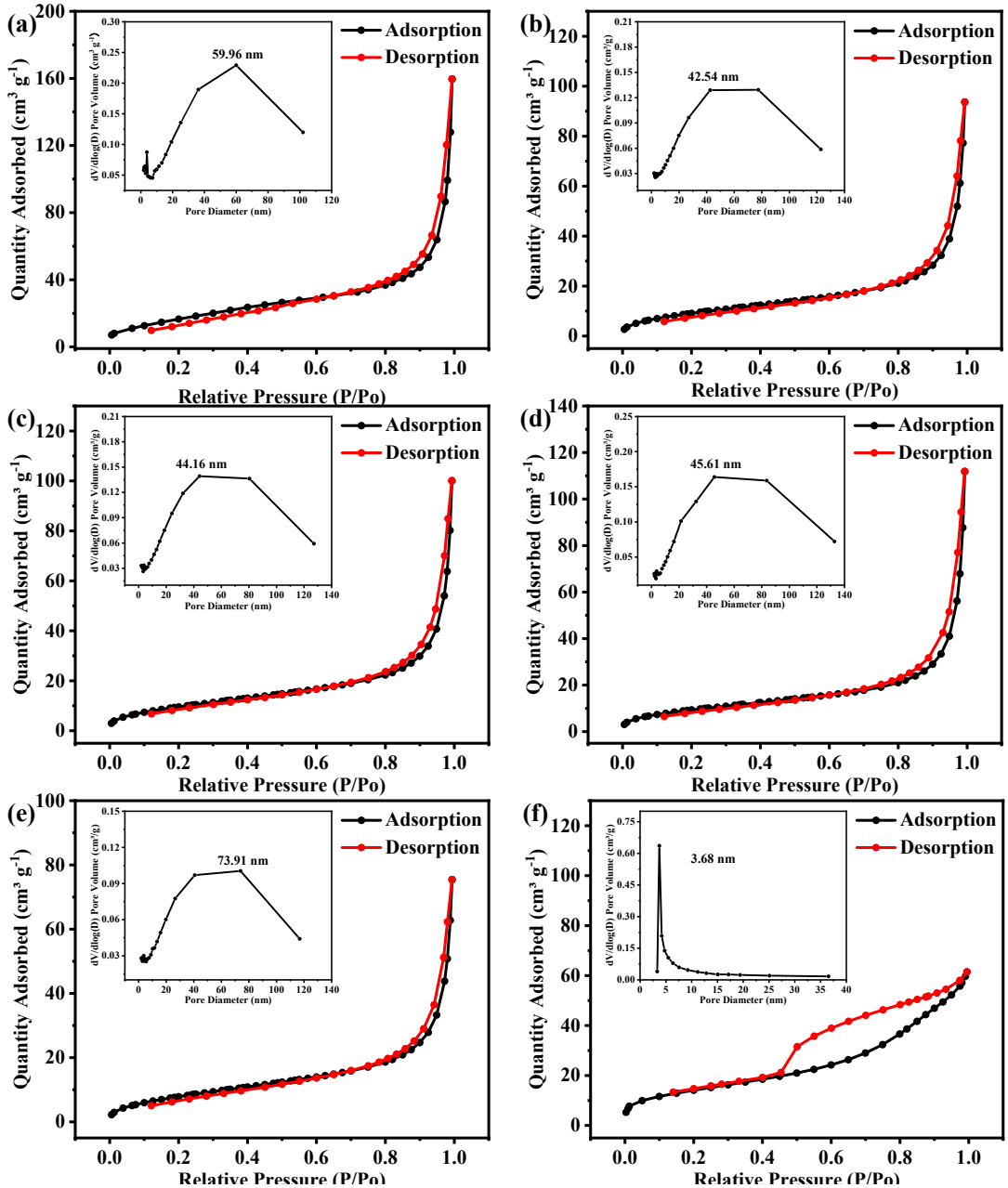

Fig. S3 N_2 adsorption–desorption isotherms at 77 K of CN (a), DBDSO/g-C_3N_4-10 (b), DBDSO/g-C_3N_4-15 (c), DBDSO/g-C_3N_4-20 (d), DBDSO/g-C_3N_4-30 (e) and DBDSO (f). Pore size distribution are shown in the insets.

Table. S1. Comparison of specific surface areas and pore size

Sample	CN	DBDSO	DBDSO/g-C_3N_4-10	DBDSO/g-C_3N_4-15	DBDSO/g-C_3N_4-20	DBDSO/g-C_3N_4-30
[a] S_{BET} ($m^2\ g^{-1}$)	66.1164	51.3616	35.5765	37.3452	35.5723	31.2482
[b] Pore size (nm)	59.96	3.68	42.54	44.16	45.61	73.91

4.1. Mott-Schottky

Moreover, according to S4, it can be seen that the flat charged positions (V_{fb}) of DBDSO and CN were -0.69 and -0.65 V (vs. Ag/AgCl), corresponding to -0.48 and -0.44 V (vs. NHE). Moreover, due to conduction band (E_{CB}) of n-type semiconductor was usually more negative 0.1−0.3 V than its flat band potential, the conduction bands (E_{CB}) of DBDSO and CN can be calculated as -0.68, -0.64 V, respectively, consistent with the data obtained through XPS-VB[S8-S9].

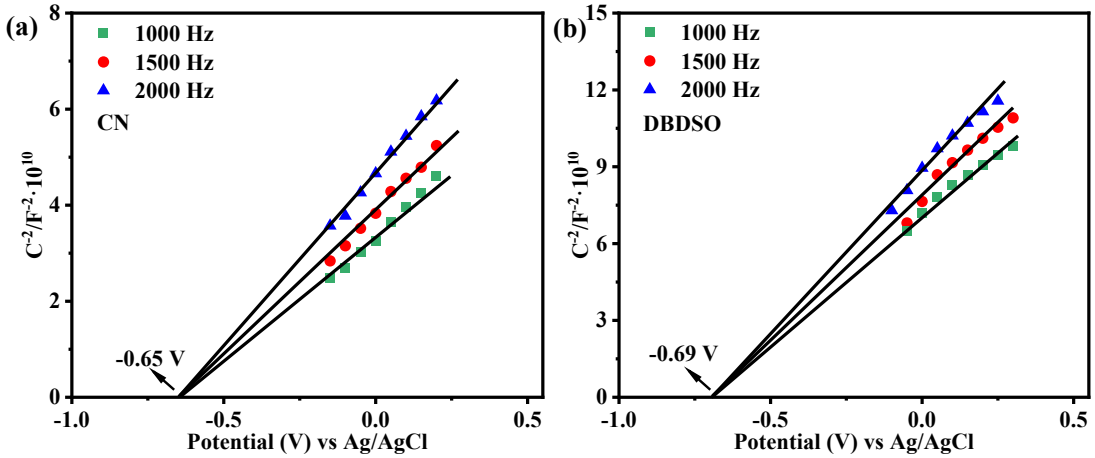

Fig. S4 Mott-Schottky plots of CN (a) and DBDSO (b) at different frequency in an aqueous solution of Na_2SO_4 (0.5 M).

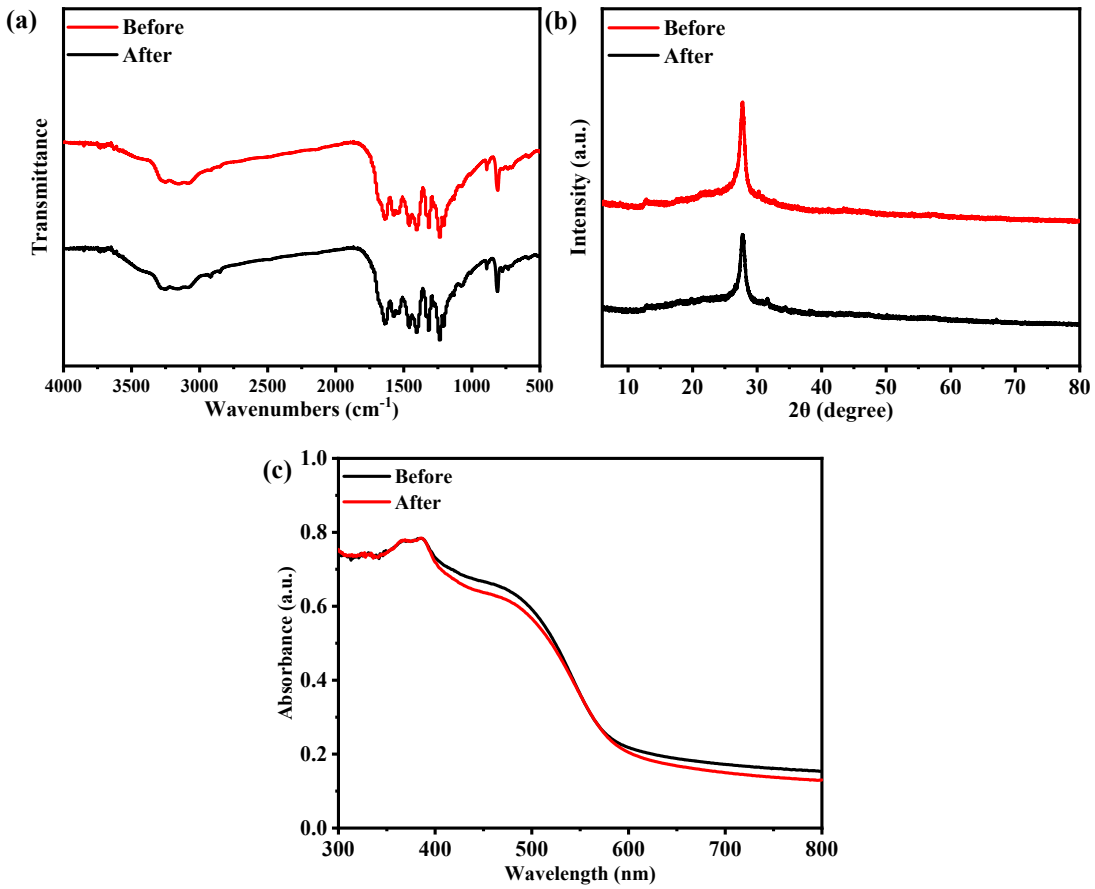

Fig. S5 FT-IR spectra (a)，XRD pattern (b), UV-Vis diffuse reflectance spectra (c) of DBDSO/g-C_3N_4-15 before and after a 15 hours of hydrogen production experiments.

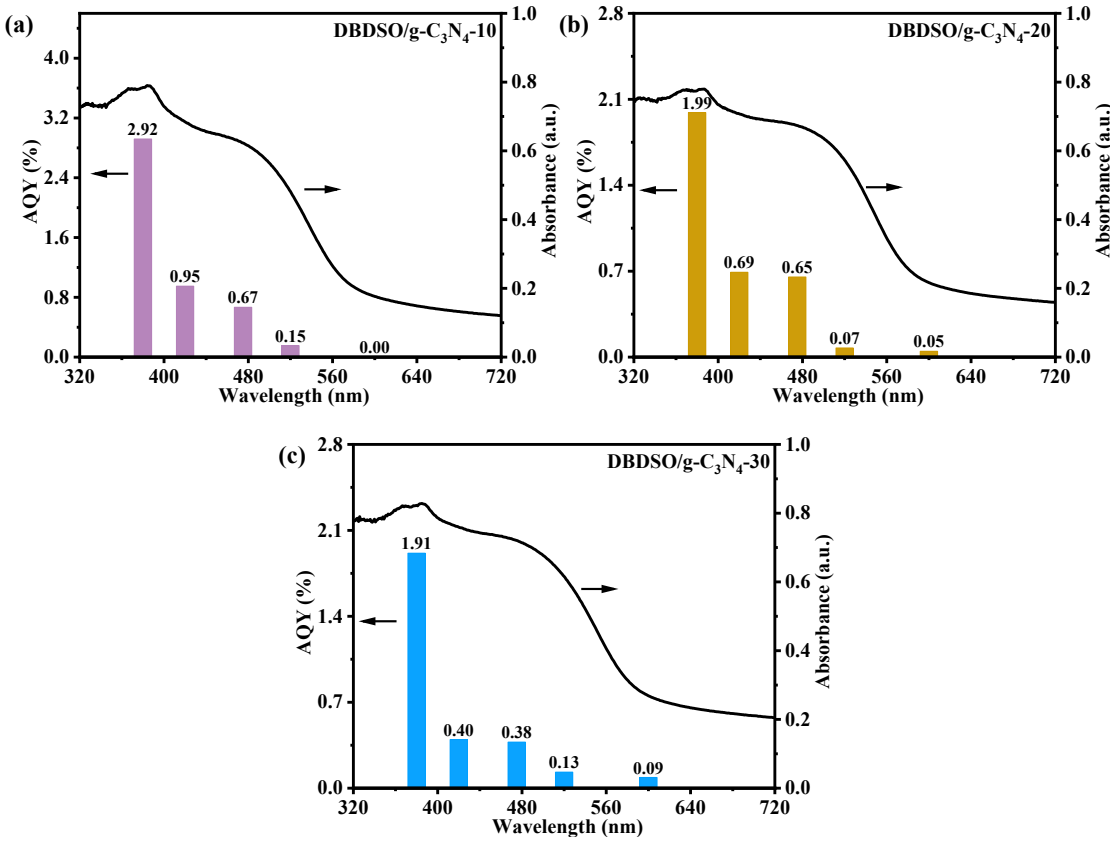

Fig. S6 Apparent quantum yield (AQY) of DBDSO/g-C_3N_4-10 (a), DBDSO/g-C_3N_4-20 (b) and DBDSO/g-C_3N_4-30 (c) at various wavelengths.

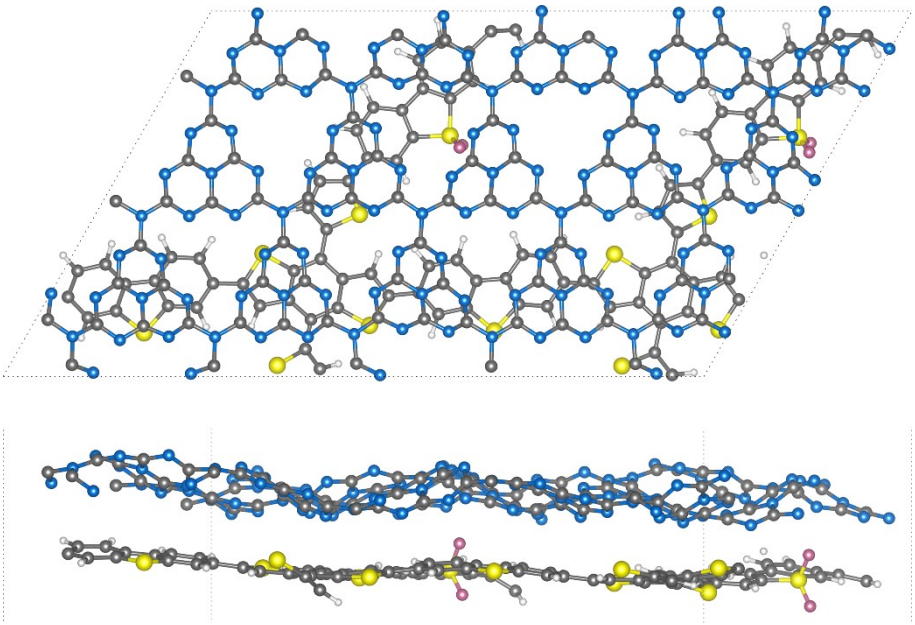

Fig. S7 Optimized structures of the constructed DBDSO/CN heterojunction models.

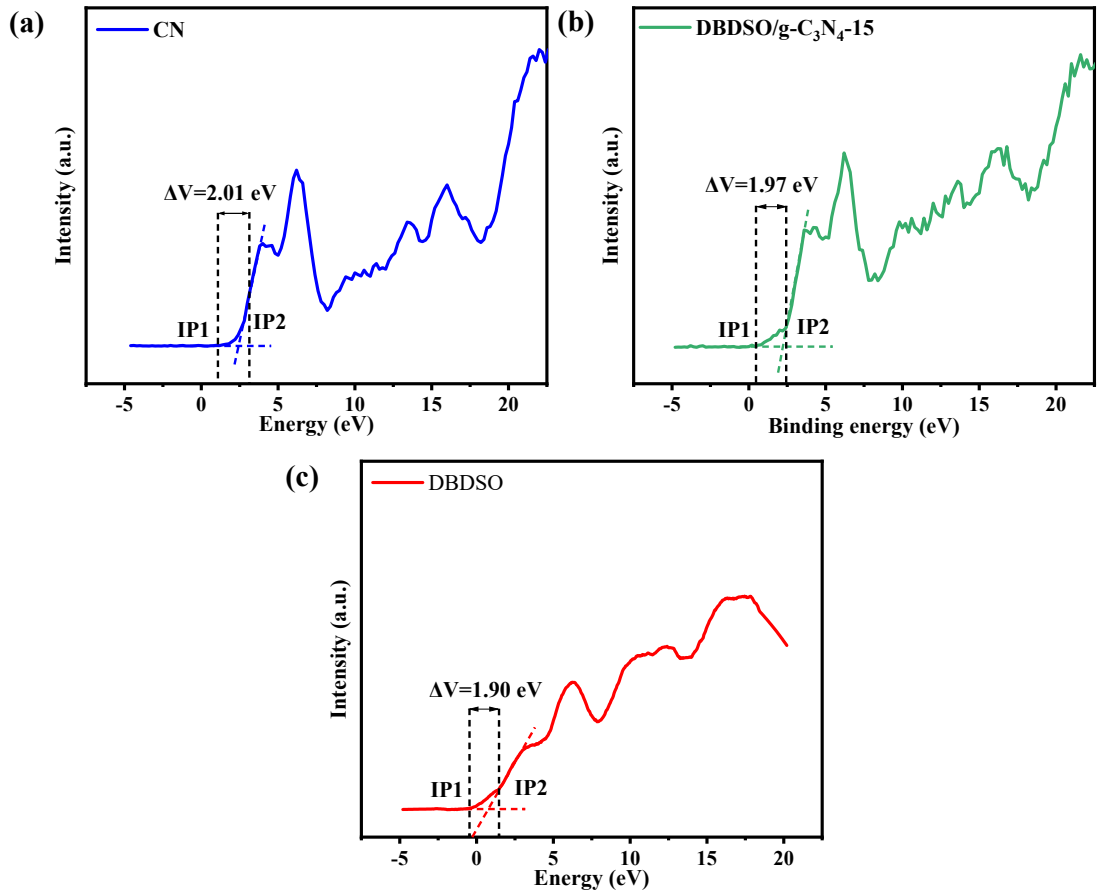

Fig. S8 XPS valance band spectras of CN (a), DBDSO/g-C_3N_4-15 (b) and DBDSO (c) at various wavelengths.

References

[S1] Y.L. Zhang, L.Q. Kong, Y. Zhang, H.M. Du, J.S. Zhao, S. Chen, Y. Xie and Y. Wang, *Org. Electron.*, 2020, **81**, 105685.

[S2] W. Huang, Q. He, Y.P. Hu and Y.G. Li, *Angew. Chem.*, 2019, **131**, 8768-8772.

[S3] C.H. Dai, S.D. Xu, W. Liu, X.Z. Gong, M. Panahandeh-Fard, Z.T. Liu, D.Q. Zhang, C. Xue, K.P. Loh and B. Liu, *Small*, 2018, **14**, 1801839.

[S4] L. Zhao, Y. Zhou, X.H. Zeng, F. Xiao, W. Fang, X. He, W.X. Li, X. Du, D.C. Wang and H. Chen, *Int. J. Hydrog. Energy*, 2023, **48**, 20290-20302.

[S5] G. Kresse, J. Furthmüller, *Phys. Rev. B*, 1996, **54**, 11169–11186

[S6] J.A. White, D.M. Bird, *Phys. Rev. B*, 1994, **50**, 4954–4957

[S7] M. Ernzerhof, G.E. Scuseria, J. Chem. Phys., 1999, **110**, 5029–5036

[S8] H.X. Shi, D.C. Feng, H.M. Li, D.S. Yu and X.D. Chen, *J. Photochem. Photobiol. A*, 2023, **435**, 114292.

[S9] W.L. Liu, Y.Q. Wang, K. Qi, Y. Wang, F.S. Wen and J.Q. Wang, *J. Alloys Compd.*, 2023, **933**, 167789.